

A test of cirrus ice crystal scattering phase functions

P. R. Field,¹ A. J. Baran,¹ P. H. Kaye,² E. Hirst,² and R. Greenaway²

Received 4 April 2003; revised 21 May 2003; accepted 24 June 2003; published 24 July 2003.

[1] In-situ ice crystal scattering has been measured in cirrus cloud with the Small Ice Detector laser scattering probe. Using light scattered from single particles (maximum dimension $\sim <100 \mu\text{m}$) at $4\text{--}10^\circ$ and $20\text{--}40^\circ$ we have tested ice crystal scattering phase functions for spheres, hexagonal columns, hexagonal plates, polycrystals an aggregate of columns and an analytic function. We find that phase functions that lack a pronounced 22° halo are the best representatives for the example data presented here. Spherical ice particle phase functions do not satisfy the measurements. **INDEX TERMS:** 0320 Atmospheric Composition and Structure: Cloud physics and chemistry; 0360 Atmospheric Composition and Structure: Transmission and scattering of radiation; 3359 Meteorology and Atmospheric Dynamics: Radiative processes. **Citation:** Field, P. R., A. J. Baran, P. H. Kaye, E. Hirst, and R. Greenaway, A test of cirrus ice crystal scattering phase functions, *Geophys. Res. Lett.*, 30(14), 1752, doi:10.1029/2003GL017482, 2003.

1. Introduction

[2] Cirrus (ice crystal) clouds have an important effect on current climate, and any changes to their characteristics will have a substantial feedback on climate change. Hence it is vital that cirrus clouds and their optical properties are well represented in climate models, see for example *Kristjansson et al.* [2000]. Field observations demonstrate that the dominating ice crystal habit found within cirrus cloud for large particles ($\sim >500 \mu\text{m}$) is ice aggregates (complex ice crystals consisting of two or more elements). For smaller ice crystals images suggest that particles are compact, but irregular (droxtals are a possible candidate, *Yang et al.* [2003]). Pristine hexagonal ice columns and ice plates are rare, see for example *Korolev et al.* [1999]. Complex ice crystals found in cirrus cloud are often modelled as hexagonal ice aggregates or polycrystals. The hexagonal ice aggregate is an arbitrary attachment of two to eight hexagonal elements, each element has a roughened surface and the aggregate has an aspect ratio (ratio of the major to minor axes of the circumscribing ellipse) close to unity, which remains invariant with size, see *Yang and Liou* [1998]. The randomized polycrystal model due to *Macke et al.* [1996] is an idealised attempt to model the effects of the more complex and irregularly shaped ice crystals found in cirrus cloud. However, in the paper by *Francis et al.* [1999] it was shown that single crystal models such as the pristine hexagonal ice column, hexagonal ice plate, polycrystal and hexagonal ice aggregate could not model radiometric

measurements at 0.87 micron between the scattering angles of about 20° to about 122° . *Gayet et al.* [1998] have also demonstrated that populations of hexagonal crystals or ice spheres are not able to reproduce the scattering phase function measured between $4\text{--}170^\circ$ with a polar nephelometer in cirrus cloud. Moreover, it was shown by *Francis et al.* [1999] that an experimentally determined phase function due to *Volkovitskiy et al.* [1980] did model more correctly the radiometric measurements. The results of *Francis et al.* [1999] suggest that a phase function that represents the single-scattering properties of an ensemble of ice crystals is more desirable. Such a phase function is called the ‘analytic’ phase function and has been previously described in *Baran et al.* [2001]. The normalized phase function is a linear piecewise extension of the Henyey-Greenstein model, which is generated from the asymmetry parameter. The analytic phase function was originally based on laboratory measurements made at $0.63 \mu\text{m}$ of the scattering phase function from a collection of non-spherical ice crystals of varying size and aspect ratio, (see *Volkovitskiy et al.* [1980]) and compares well with laboratory measurements of complex ice analogues at $0.49 \mu\text{m}$ (*Ulanowski et al.*, 2003).

[3] The aim of this paper is to test which scattering phase functions are most applicable to a measured population of natural ice particles (maximum size $<100 \mu\text{m}$). This will be done by assuming that we are observing randomly oriented individual ice crystals at a non-absorbing wavelength, and concentrating on scattering of incident radiation forward of 40° . Previous papers tend to concentrate on testing phase functions at larger side or backscattering angles [*Baran et al.*, 2001].

2. Method

[4] Using scattered light (532 nm) collected at $4\text{--}10^\circ$ and $20\text{--}40^\circ$ from individual particles we have tested 11 scattering phase functions. The scattered light was collected with the Small Ice Detector [*Hirst et al.*, 2001]. SID is a laser scattering device that can count and size spherical particles between 2 and $50 \mu\text{m}$ (diameter) and count non-spherical particles. The probe uses six detectors arranged azimuthally at a forward scattering angle of 30° (detector half-angle of 10°), with a seventh detector mounted at the forward scattering angle. Since our measurements cover angles that include the 22° halo it is expected that we should be able to distinguish between phase functions with and without this feature. One of the six 30° detectors has an iris fitted to allow it to define a $400 \times 800 \mu\text{m}$ ellipse on the scattering laser. When light was detected by this detector and one other detector, a particle was known to be in the sample volume and the detector responses were recorded. By comparing the responses of the azimuthally arranged detectors an ‘asphericity factor’ (A_f) could be obtained for each particle measured that ranges from 0 for spherical

¹Met Office, Exeter, UK.

²STRC, University of Hertfordshire, UK.

particles to 100 for very non-spherical particles (see *Hirst et al.* [2001] for more details). In this study we compare the average response of the five circular ‘30°’ detectors without an iris to the annular, 4–10° forward scattering angle detector. By comparing the relative response of the forward and ‘30°’ detectors in liquid and ice conditions we can test the expected response of the candidate scattering phase functions. Because of uncertainties in particle orientation and phase function it is difficult to size ice crystals, but the SID will probably be detecting ice crystals up to $\sim 100 \mu\text{m}$ before the detectors saturate and the particle is ignored. For the data presented in this paper the SID was flown aboard the UK C-130 aircraft.

[5] Figure 1 shows the normalised scattering phase functions for randomly oriented particles. The scattering functions were generated assuming an incident light wavelength of $0.55 \mu\text{m}$ using improved geometric optics for columns (maximum dimension, d_m , 25 and $7.5 \mu\text{m}$; aspect ratio 1.429), plates (maximum dimensions 25 and $7.5 \mu\text{m}$; aspect ratios 0.343 and 0.665, respectively) and aggregates of columns [*Yang and Liou*, 1996]. The scattering function for the aggregate of columns is invariant with size. The polycrystal scattering function was calculated using ray-tracing for a particle with a $25 \mu\text{m}$ maximum dimension [*Macke*, 1996]. An analytic phase function proposed by *Baran et al.* [2001] using an asymmetry parameter of $g = 0.76$ (the choice of other g values will be commented upon later) and the calculated curve from Mie theory for a $10 \mu\text{m}$ radius sphere (smoothed for clarity) are also shown. The grey shaded areas mark the range of scattering angles covered by the SID probe.

[6] The energy scattered per unit time to the forward (4–10°) detector E_c and to one 30° detector E_{30} is

$$E_c = \frac{I_0 C_{sca}}{4\pi} \int_c P(\theta) d\Omega \quad (1)$$

$$E_{30} = \frac{I_0 C_{sca}}{4\pi} \int_{30} P(\theta) d\Omega \quad (2)$$

where I_0 is the in intensity of the incident light, C_{sca} is the scattering cross section of the particle, $P(\theta)$ is the scattering phase function and $d\Omega$ is the solid angle element. The subscript on the integral signs indicate integration over the solid angle relevant for the central 4–10° detector (c) and 30° detector (30). Thus if we apply a constant factor, k , that is independent of particle size to account for the variation in gains between the 4–10° and 30° detectors in the SID we can combine equations (1) and (2) to obtain the theoretical detector ratio, TDR

$$TDR = k \frac{E_{30}}{E_c} = k \frac{\int_{30} P(\theta) d\Omega}{\int_c P(\theta) d\Omega} \quad (3)$$

that can be directly compared with the measured detector ratio, MDR.

$$MDR = \frac{D_{30}}{D_c} \quad (4)$$

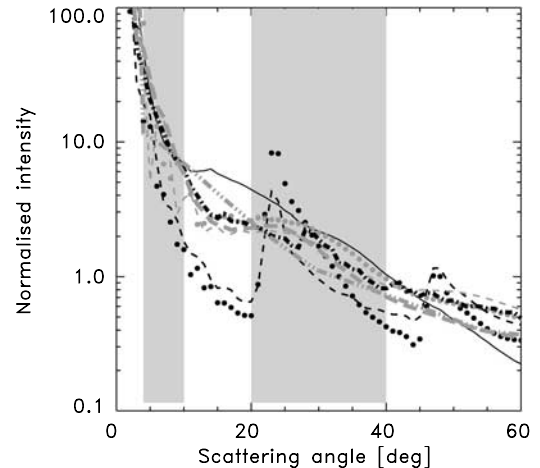


Figure 1. Normalised randomly oriented phase functions for $10 \mu\text{m}$ (radius) spheres (solid), column ($7.5 \mu\text{m}$, grey dots; $25 \mu\text{m}$ black dots), plate ($7.5 \mu\text{m}$, grey dash; $25 \mu\text{m}$ black dash), polycrystal (dot-dash), aggregate (thin grey dash) and analytic (dot-dot-dot-dash). The shaded regions mark the scattering angles covered by the SID probe.

where D_{30} and D_c are the 30° and 4–10° detector signals, respectively.

[7] Using data obtained from sampling droplets we will find k empirically so that we can compare the response of the SID detectors in ice conditions to various phase functions.

3. Data

[8] The reference liquid case used to show the response to spheres was taken from two 60 km runs in stratocumulus cloud that had a mode in droplet size at $10 \mu\text{m}$ in radius and concentrations of $75(\pm 23) \text{ cm}^{-3}$ (1 Hz). The detector response from droplets with radii between 2.5 and $16 \mu\text{m}$ were used in the analysis.

[9] The ice runs used to test the phase functions are taken from two ~ 50 km runs in cirrus. The ice crystal data were obtained at temperatures of -43C and -46C in cirrostratus to the north of Scotland (17 October 2000). The size distribution of larger particles was narrow with the 2D-C optical array probe indicating an absence of particles larger than $600 \mu\text{m}$. The 2D images appeared irregular and compact, but it should be borne in mind that the crystals being sampled by the SID probe are smaller ($< 100 \mu\text{m}$) than those that can be accurately discerned by the 2D-C probe. SID concentrations (1 Hz) along these runs varied between 0.5 and 3 cm^{-3} while the Forward Scattering Spectrometer Probe (FSSP) concentrations (1 Hz) tended to be a factor of 5 lower. This difference is attributed to the different sensitivities of the probes. *Field et al.* [2003] have shown with a fast FSSP that the distribution of ice particle interarrival times can be bimodal with modes at 10^{-4} and 10^{-2} s. It is unclear whether the particles associated with the short interarrival time mode are a result of ice crystals breaking up on the probe inlet. If ice particles are shattering on the inlet of the FSSP then the same could be true for the SID probe. To avoid this uncertainty we have chosen two

runs where particles with the short interarrival time were largely absent.

4. Results and Discussion

[10] Using the stratocumulus data we have selected collections of droplets with narrow size ranges to compare the TDR for water spheres with the measured Detector Ratio (MDR). The SID particle sizing is done using the light scattered to the 30° detectors and is only appropriate for water spheres. The droplet radii used were $3\ \mu\text{m}$ (range $2.5\text{--}3.5\ \mu\text{m}$, 5347 droplets), $5\ \mu\text{m}$ (range $4.5\text{--}5.5\ \mu\text{m}$, 16367 droplets), $10\ \mu\text{m}$ (range $9\text{--}11\ \mu\text{m}$, 67888 droplets) and $15\ \mu\text{m}$ (range $14\text{--}16\ \mu\text{m}$, 19423 droplets). Using equation 3 we adjusted k until satisfactory agreement between the peaks in the histograms of MDR and TDR was achieved for these four monodisperse distributions. Figure 2 shows the result of this exercise using the chosen value of $k = 105$. In theory we would expect delta functions from the histograms of MDR for droplets, but variance will arise through noise in the optics and differences in droplet sizes. The four MDR peaks show good agreement with the TDRs, indicating that the SID droplet size calibration is correct. The smaller droplets have smaller MDRs indicating that relatively more light is scattered to the forward direction as the droplets get smaller, as expected. Once the value of k was found the TDRs for the non-spherical particles could then be computed (see Table 1).

[11] For the data obtained in the cirrus cloud we again attempted to size sort the particles. As stated above, the size attributed to each ice particle is based on a calibration for water spheres and will be inaccurate when applied to different shapes. The reason we chose to do this was because if the ice particles are spherical then the MDRs should behave in a similar way to the water case and display peaks located at TDR values indicated in Table 1 for water spheres. Figure 3 shows the MDRs for the ice

Table 1. Theoretical Detector Ratio (TDR) Responses for Different Phase Functions

Phase function type	TDR	d_m [μm]	g
Sphere	8.8	30.0	0.86
Sphere	8.1	20.0	0.85
Sphere	6.3	10.0	0.84
Sphere	4.2	6.0	0.82
Hexagonal column	18.3	25.0	0.81
Hexagonal column	5.8	7.5	0.70
Hexagonal plate	8.8	25.0	0.87
Hexagonal plate	6.7	7.5	0.68
Polycrystal	4.9	25.0	0.74
Column aggregate	3.8	25.0	0.76
Analytic	5.1	25.0	0.76

The crystal maximum dimension, d_m , and the asymmetry parameter, g , are also given.

particles with *indicated* radii of $3\ \mu\text{m}$ (range $2.5\text{--}3.5\ \mu\text{m}$, 1499 particles), $5\ \mu\text{m}$ (range $4.5\text{--}5.5\ \mu\text{m}$, 3552 particles), and $10\ \mu\text{m}$ (range $9\text{--}11\ \mu\text{m}$, 782 particles). The resulting MDR histograms are much broader than for the water case and are very similar to each other. They all have a peak in the MDR histogram located between $5.0\text{--}6.5$. The fact that the peaks in the histograms of the MDRs for these nominal size ranges do not correlate with the TDRs for the same size spheres indicates that the sphere phase function is not appropriate for these cirrus ice crystals. We have also found that prolate spheroids (aspect ratio 3:2) show a size dependent TDR (not shown here for brevity) and so will not fit these observations of MDR. The non-spherical particle phase functions that satisfy the measurements are the $7.5\ \mu\text{m}$ column, $7.5\ \mu\text{m}$ plate, the analytic function and the polycrystal. These phase functions lack a strong 22° halo unlike the larger plate and column particles. Although the aggregate of columns also has a featurless phase function the TDR it generates is too small to match the observations.

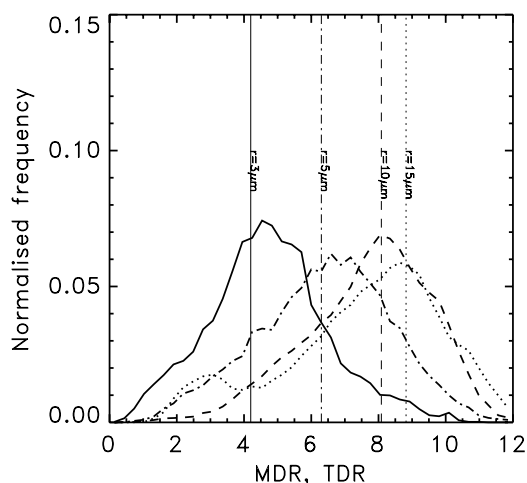


Figure 2. Histograms of the Measured Detector Ratio for ensembles of droplets with radii $3\ \mu\text{m}$ (range $2.5\text{--}3.5\ \mu\text{m}$, 5347 droplets, solid line), $5\ \mu\text{m}$ (range $4.5\text{--}5.5\ \mu\text{m}$, 16367 droplets, dot-dash line), $10\ \mu\text{m}$ (range $9\text{--}11\ \mu\text{m}$, 67888 droplets, dash line), $15\ \mu\text{m}$ (range $14\text{--}16\ \mu\text{m}$, 19423 droplets, dotted line). The theoretical detector ratios for water spheres are marked with vertical lines and annotated.

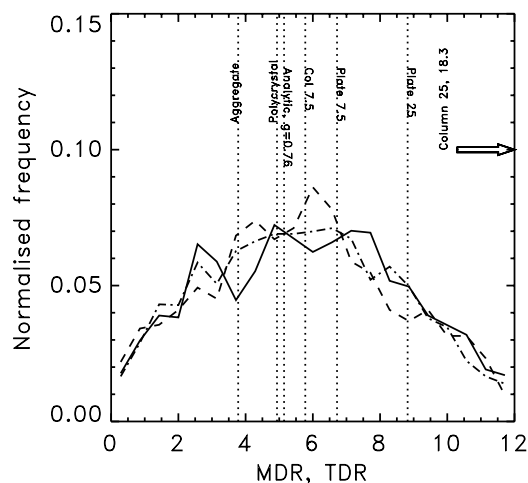


Figure 3. Histograms of the Measured Detector Ratio for ensembles of particles with indicated radii, assuming spherical geometry, $3\ \mu\text{m}$ (range $2.5\text{--}3.5\ \mu\text{m}$, 1499 particles, solid line), $5\ \mu\text{m}$ (range $4.5\text{--}5.5\ \mu\text{m}$, 3552 particles, dot-dash line), $10\ \mu\text{m}$ (range $9\text{--}11\ \mu\text{m}$, 782 droplets, dash line). The theoretical detector ratios for different particle shapes and sizes are marked with vertical lines and annotated.

It is also noted here that the choice of $g = 0.76$ for the analytic function gives good results. Choosing other values of g generates TDRs from the analytic function ranging from 12.8 for $g = 0.6$ to 1.3 for $g = 0.95$.

[12] Over the size ranges considered, the analytic, polycrystal and aggregate functions do not vary considerably with particle size. Although, the indicated size is not applicable to non-spherical particles, presumably the relative progression from smaller to larger particles is still a valid assumption. If so then we can speculate that, in the size range detectable by the SID probe, the phase functions appear to be unaffected by particle size.

[13] The TDR is not a unique property of a phase function (e.g. TDR of 25 μm hexagonal plate = TDR of 30 μm sphere). Hence, many more phase functions that lack a dominant halo feature could also satisfy the observations (e.g. a column with inclusions, *Labonnote et al.* [2000], distorted hexagonal columns, *Knap et al.* [1999]). We are unable to discriminate further between the phase functions and we note that further observations involving larger scattering angles (e.g. *Gayet et al.* [1998]) and other radiometric data are required.

[14] Problems which may effect these results are the possible shattering of ice crystals on the inlet prior to sampling in the instrument and the orientation of particles in the SID inlet tube. The shattering problem has been mentioned above and should have been avoided by the choice of data used here. The orientation of particles by the probe inlet tube would lead to changes in the column and plate detector ratios only. In the worst case the columns would be aligned perpendicular to the signal laser and so enhance the halo effect. For the plates the worst case would be that they would align face-on to the signal laser and so scatter very little light to the '30°' detectors.

5. Conclusion

[15] Using in-situ scattering data from ice crystals in cirrus and droplets in stratocumulus cloud we have compared the relative scattering responses of cirrus particles $\sim < 100 \mu\text{m}$ at 4–10° and 20–40°. Bearing in mind potential problems arising from orientation of particles in the airflow through the probe, the most realistic candidate phase functions are those that lack a significant halo feature such as the 7.5 μm column, 7.5 μm plate, the analytic function and the polycrystal. The sphere phase function is not applicable to these cirrus ice particles.

[16] **Acknowledgments.** The authors wish to thank the staff of the Meteorological Research Flight and the C-130 RAF aircrew. We also wish to thank Phil Brown, Pete Francis and two anonymous reviewers for valuable comments that helped improve this manuscript.

References

- Baran, A. J., P. N. Francis, L. C. Labonnote, and M. Doutriaux-Boucher, A scattering phase function for ice cloud: Tests of applicability using aircraft and satellite multi-angle multi-wavelength radiance measurements of cirrus, *Quart. J. Roy. Meteorol. Soc.*, 127, 2395–2416, 2001.
- Field, P. R., R. Wood, P. R. A. Brown, P. H. Kaye, E. Hirst, R. Greenaway, and J. A. Smith, Ice particle interarrival times measured with a fast FSSP, *J. Atmos. Ocean. Technol.*, 20(2), 249–261, 2003.
- Francis, P. N., J. S. Foot, and A. J. Baran, Aircraft measurements of the solar and infrared radiative properties of cirrus and their dependence on ice crystal shape, *J. Geophys. Res.*, 104, 31,685–31,695, 1999.
- Gayet, J.-F., F. Auriol, S. Oshchepkov, F. Schroder, C. Duroure, G. Febvre, J.-F. Fournol, O. Crepel, P. Personne, and D. Daugeron, In-situ measurements of the scattering phase function of stratocumulus, contrails and cirrus, *Geophys. Res. Lett.*, 25(7), 971–974, 1998.
- Hirst, E., P. H. Kaye, R. S. Greenaway, P. R. Field, and D. W. Johnson, Discrimination of micrometre-sized ice and super-cooled droplets in mixed-phase cloud, *Atmos. Environ.*, 35, 33–47, 2001.
- Knap, W. H., M. Hess, P. Stammes, and R. B. A. Koelemeijer, Cirrus optical thickness and crystal size retrieval from ATSR-2 data using phase functions of imperfect hexagonal ice columns, *J. Geophys. Res.*, 104(D24), 31,721–31,730, 1999.
- Korolev, A. V., G. A. Isaac, and J. Hallett, Ice particle habits in Arctic clouds, *Geophys. Res. Lett.*, 26(9), 1299–1302, 1999.
- Labonnote, L. C. G. Brogniez, M. Doutriaux-Boucher, and J.-C. Buriez, Modelling of light scattering in cirrus clouds with inhomogeneous hexagonal monocrystals. Comparison with in-situ and ADEOS-POLDER measurements, *Geophys. Res.*, 113–116, 2000.
- Kristjansson, J. E., J. M. Edwards, and D. L. Mitchell, The impact of a new scheme for the optical properties of ice crystals on the climate of two GCMs, *J. Geophys. Res.*, 105, 10,063–10,079, 2000.
- Macke, A., J. Mueller, and E. Raschke, Single scattering properties of atmospheric ice crystals, *J. Atmos. Sci.*, 53, 2813–2825, 1996.
- Ulanowski, Z., E. Hesse, P. H. Kaye, A. J. Baran, and R. Chandrasekhar, Scattering of light from atmospheric ice analogues, *J. Quantit. Spectr. Rad. Transf.*, 79–80, 1091–1102, 2003.
- Volkovitskiy, O. A., L. N. Pavlova, and A. G. Petrushin, Scattering of light by ice crystals, *Atmos. Ocean. Phys.*, 16, 90–102, 1980.
- Yang, P., and K. N. Liou, Single-scattering properties of complex ice crystals in terrestrial atmosphere, *Contrib. Atmos. Phys.*, 71, 223–248, 1998.
- Yang, P., and K. N. Liou, Geometric-optics-integral-equation method for light scattering by non-spherical ice crystals, *Appl. Opt.*, 35, 6568–6584, 1996.
- Yang, P., B. A. Baum, A. J. Heymsfield, Y. X. Hu, H.-L. Huang, S.-C. Tsay, and S. Ackerman, Single scattering properties of droxtals, *J. Quantit. Spectr. Rad. Transf.*, 79–80, 1159–1169, 2003.

A. J. Baran and P. R. Field, Met Office, Exeter, UK. (paul.field@metoffice.com)

R. Greenaway, E. Hirst, and P. H. Kaye, STRC, University of Hertfordshire, UK.